Hierarchical Molybdenum Nitride Nanochexes by a Textured Self-Assembly in Gas–Solid Phase for the Enhanced Application in Lithium Ion Batteries

Haitao Xu,[†] Huijuan Zhang,[†] Ling Fang,[†] Jiao Yang,[†] Kai Wu,[*,‡] and Yu Wang[*,†]

[†]The State Key Laboratory of Mechanical Transmissions and School of Chemistry and Chemical Engineering, Chongqing University, Chongqing 400044, China and [‡]Beijing National Laboratory for Molecular Sciences, College of Chemistry and Molecular Engineering, Peking University, Beijing 100871, P.R. China

ABSTRACT Self-assembly, as one kind of general phenomenon, has often been reported in solution chemistry. However, in gas–solid phase, it seldom has been disclosed. The MoN nanochex exhibits unique geometrical shape. Its body segment is composed of textured single crystal MoN nanowires, while its edges parallel to [$\bar{1}2\bar{2}$] direction are attached by nanowires whose crystal orientation is different from that of the body segment. In this paper, the structure of the MoN nanochex is studied, and accordingly, a possible growth mechanism is proposed. We expect to extend this method to designed synthesis of many other functional materials, such as nitrides, carbides, and borides, and thereby to significantly tailor their resulting properties. Meanwhile, as one promising electrode material for Li-ion batteries (LIBs), MoN nanochex on Ti foil has been applied in the electrochemical energy storage, and stably delivered a specific capacity of 720 mAh/g with a remarkable Coulombic efficiency up to 98.5%, implying an achieved synergic effect derived from both mesoporous structure and the direct contact with the conducting substrate.

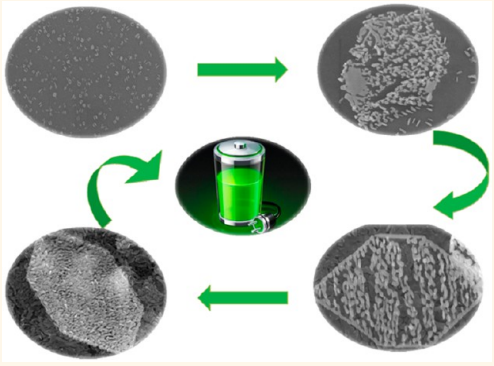

KEYWORDS: self-assembly · nanochexes · Li-ion batteries · anode · MoN

In the past few decades, extensive efforts have been placed on synthesis of 1-D nanostructures, such as nanotubes, nanowires, nanorods, and nanobelts, owing to their unique applications in mesoscopic physics and the fabrication of nanoscale devices.[1–5] Meanwhile, synthesis of hierarchical nanostructures with controllable sizes, shapes, and compositions has stimulated great research interest in recent years. As is well-known, conjunction and integration of the self-assembly process and structures are the key to bridging the "bottom-up" with the "top-down" approach in future nanotechnology. In this field, much work has been done to realize the dream of fabricating hierarchical nanostructures.[6–14] For example, CuO, ZnO "dandelions" were obtained by self-assembly or Kirkendall process in solution,[15,16] Hydrophobic interaction, DNA hybridization, and a Langmuir–Blodgett technique, and so on, have been utilized to fabricate some kinds of self-assembly uniform nanorods.[17–19] Meanwhile, biomaterials-like morphologies have been synthesized *via* self-assembled mesophase materials using solution-based chemical approaches.[20,21] To date, structures formed by self-assembly of size- and shape-controlled nanocrystals, passivated with surfactant and suspended in solution, have been demonstrated for a wild range of metallic, semiconductor, and oxide nanocrystals.[22–24] However, integration of 1-D nanoscale building blocks into two- and three-dimension (2D/3D) ordered superstructures or complex functional architectures still remains a significant challenge. One of the most important reasons is that, except for some oxides,[8–13] for example, ZnO, In_2O_3, SnO_2, there are few reports about other materials concerning the self-assembly of nanosheets or other nanostructures into hierarchical functional structures in gas–solid phase.

* Address correspondence to wangy@cqu.edu.cn, kaiwu@pku.edu.cn.

Received for review November 9, 2014 and accepted May 20, 2015.

Published online May 20, 2015
10.1021/acsnano.5b02415

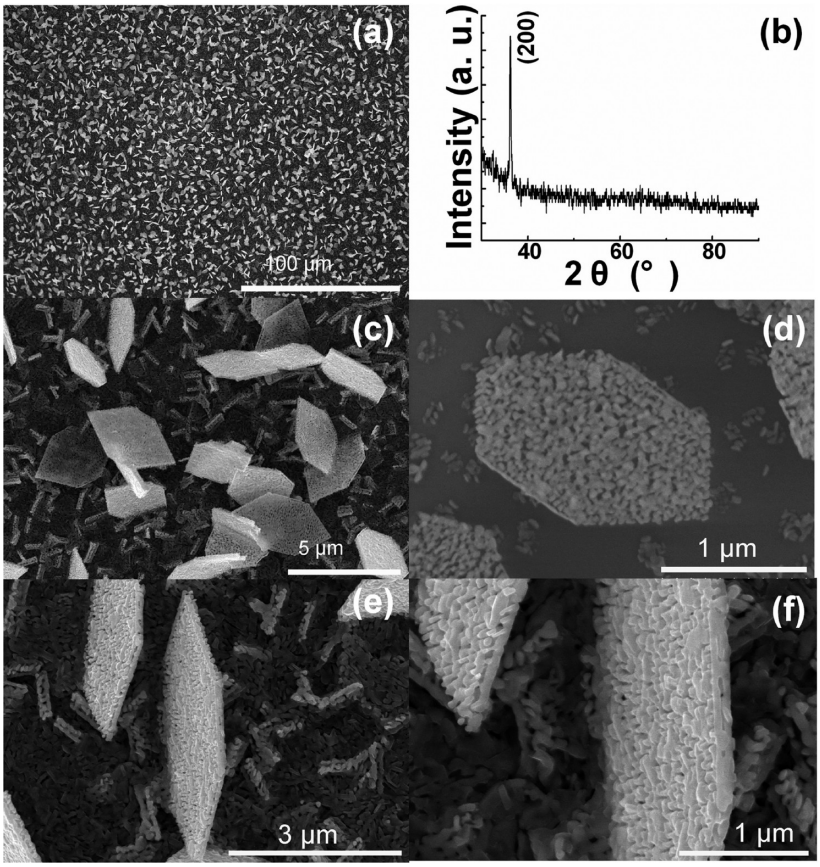

Figure 1. (a) A typical low-magnification SEM image of the as-synthesized hexagon-like MoN nanostructure distributed uniformly on the Ti foil surface, showing high controllability of the process; (b) XRD patterns of the products shown in (a), which is indexed to hexagonal phase MoN; (b–f) high-magnification SEM images of MoN nanostructure, showing the detailed information about the products.

On the other hand, in nanomaterials research fields, great attention has been paid to transition-metal nitrides, which are famous for possessing many special physical and chemical properties, such as excellent hardness, high melting point, great catalytic activity and selectivity, and superconductivity.[25] These properties are favorable for their applications in many fields. Especially, MoN, for its attractive mechanical, electrical, magnetic properties and wonderful heterogeneous catalytic activity in many aspects, such as ammonia synthesis,[26] hydrodenitrogenation (HDN),[27] hydrodesulfurization (HDS),[28,29] and isomerization of certain hydrocarbons,[30,31] is suitable for applications in cutting tools, wear-resistant parts, high temperature materials and superconductors.[26−31] Until now, MoN has been synthesized mainly by several ways, for example, ion beam assisted deposition, reactive sputtering, ion implantation, and multiple laser irradiation.[32−36] However, except for nanorods, nanoparticles, and films, other MoN nanostructures have seldom been fabricated.[26−36]

In this work, for the first time, we report a novel self-assembled molybdenum nitride (MoN) nanochex with morphology of compressed hexagon, which is synthesized by a new self-assembly way named "self-confinement process". The nanochexes exhibit unique geometrical shapes, and their body segments are composed of far-flung MoN nanosheets or nanowires. Moreover, these nanosheets or nanowires show the same crystal orientation and are connected or melted into an integrated one. Interestingly, along the [$\bar{1}2\bar{2}$] direction of the hexagon-like nanostructure, there exist two MoN nanowires, whose crystal orientation is apparently different from their body segment. As for the mechanism of this complex nanostructure's growth, a couple of processes have been considered. In this paper, structure of the products is analyzed. Growing process and formation mechanism are traced and investigated. At the same time, a new concept, so-called "self-confinement process" is raised. Finally, MoN nanochexes have successfully been applied in lithium ion batteries (LIBs) anode, indicating high capacity, enhanced rate capability, and cycling ability.

RESULTS AND DISCUSSION

In a typical synthesis, a lot of products are observed on the applied Ti foil (Figure 1a). This process has a very high repeatability if the procedure is followed as described in the experimental section. A closer investigation of the products in Figure 1a indicates that they

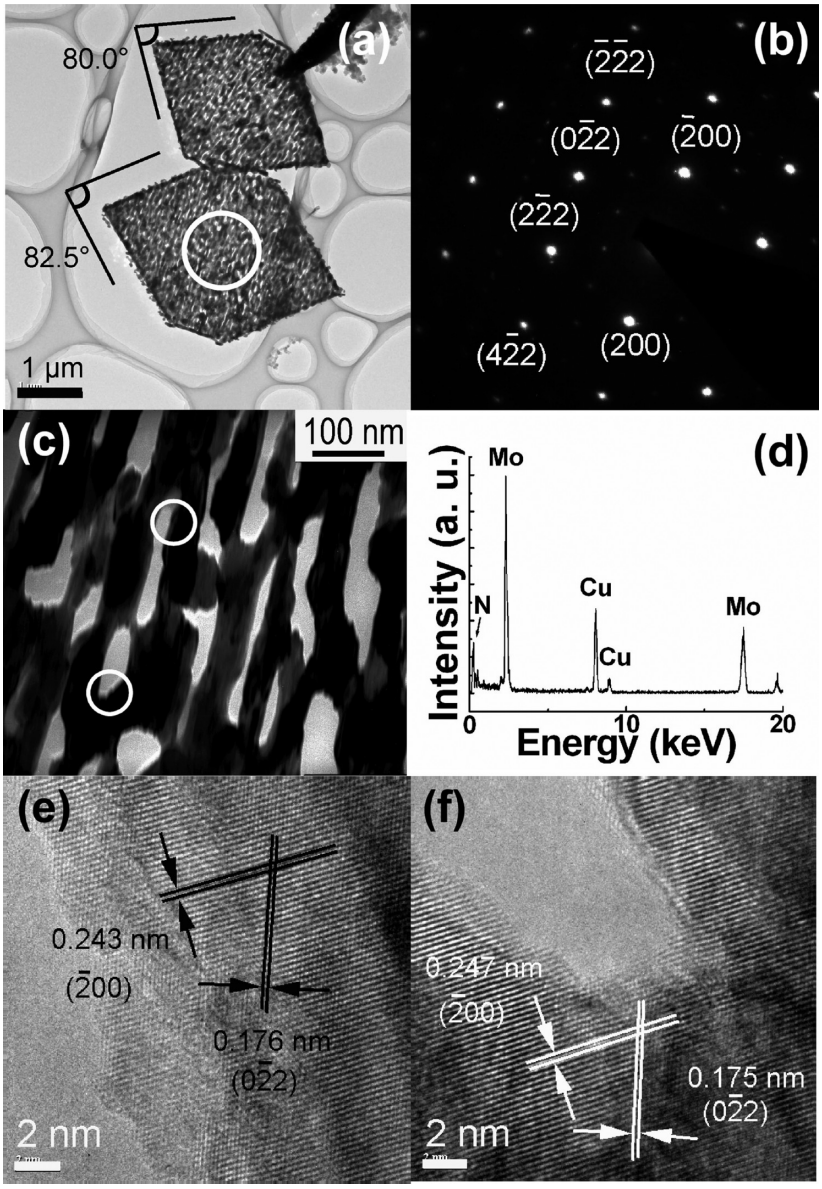

Figure 2. (a) Bright-field TEM image of the hexagon-like MoN nanostructure, and the acute angle in the front side of the products is depicted. (b) SAED pattern of the nanostructure marked with a circle in (a). (c) A closer examination about (a) shows that the body-portion of products actually is an indivisible one. (d) EDS spectrum of body-portion shown in (c). (Cu signal comes from the TEM Cu grid.) (e and f) HRTEM images of location circled in (c) show the fairly good crystal fringes which are indexed to hexagonal phase MoN.

are mostly hexagon-like structures as presented in the enlarged image (Figure 1c), and we can call them "nanochexes". The corresponding XRD data is shown in Figure 1b. We could find that there is only one diffractive peak which can be indexed to pure MoN in hexagonal phase (JCPDS, 25-1367; space group, $P6_{3/mmc}$). No strongest peaks from other impurities can be detected from the XRD diagram, suggesting that our samples have high purity and, meanwhile, demonstrate fairly good crystal orientation.

From the samples dispersed on Ti foil, we could see that MoN particles have an average size of about 1−4 μm and apparently there is a difference between ideal hexagon and the nanochex. The longer width is about 2−4 μm; however, the shorter one is about 1−3 μm. Also we could find out that these samples, in fact, are composed of some regularly textured nanostructures and have some interspaces among them. These observations are confirmed in our following transmission electron microscopy (TEM) analyses. Scanning electron microscopy (SEM) images in Figure 1d,e disclose the front and flank of nanochexes. Especially from the enlarged image (Figure 1f) in Figure 1e, thickness of the samples is estimated to be 100−150 nm.

To investigate the detailed information about the acquired nanochexes, we collected correlative data as shown in Figure 2. Figure 2a is the normal TEM image, and Figure 2b is its corresponding selected area

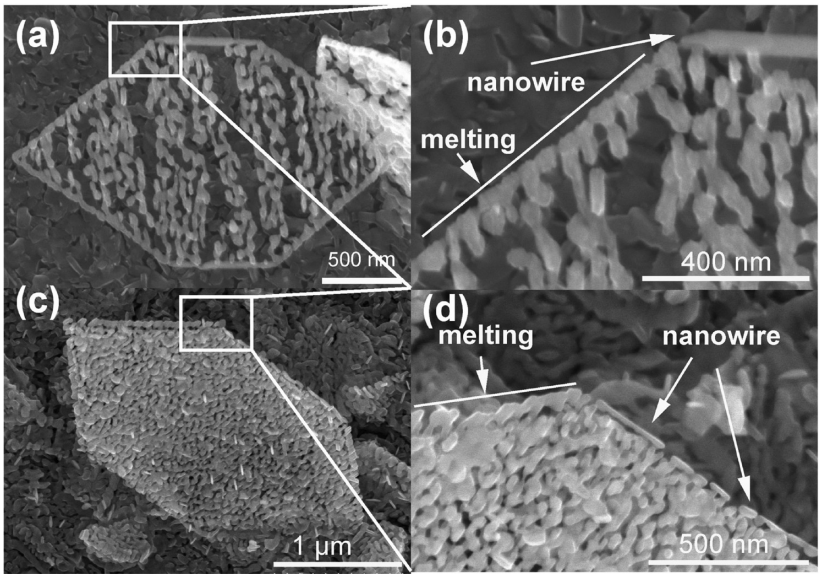

Figure 3. SEM images of hexagon-like MoN nanostructure are shown to reveal that MoN nanowires grow along the destined direction. Panels b and d are separately the enlarged pictures for panels a and c, respectively.

electron diffraction pattern (SAED). Interestingly, SAED indicates that the nanochexes have a "single crystalline" feature. On the basis of the diffraction spots in Figure 2b and elemental analysis by energy-dispersive X-ray spectrum (EDS, Figure 2d), calculation of crystal spacing constants reveal that the nanochexes are single crystal MoN in hexagonal phase, which matches very well with the XRD data (the Cu signal of EDS comes from the TEM grid). The front crystal plane of the MoN nanochex is (011) and the direction parallel to the compressed side is $[\bar{1}2\bar{2}]$. The direction perpendicular to the compressed side, that is to say, along the nanosheets or nanowires growth direction, is [200]. It is surprising that all acute angles for the nanochexes have been centralized from 80° to 84°. Is it occasional or inevitable? Detailed analysis and deduction will be described in a later section.

Figure 2a is magnified and the closer observation is shown in Figure 2c, where it is disclosed that the whole segment has been integrated together into an indivisible one. The microstructure of the MoN nanochex is further investigated by high-resolution TEM (HRTEM) imaging. The lattice fringes of selected area (circled in Figure 2c) with regular crystal spacing of 0.243 nm isare indexed to $(\bar{2}00)$ planes of hexagonal phase MoN, while the other lattice fringes of 0.176 nm are consistent with the interplanar spacing of $(0\bar{2}2)$ planes. The well-resolved fringes and the crystal structure's perfect transition between two neighboring nanowires (Figure 2f) further confirm the single crystallinity of MoN nanochex. In addition, the oriented nanowires have small diameter of tens of nanometers, implying the obtained nanochexes have high specific surface areas. As is well-known, high specific surface area is indispensable to catalysts, and at the same time, the crystallinity of catalyst is another crucial factor to greatly improve the catalytic performance in most cases. Combined with these two aspects, the as-synthesized MoN nanochex maybe has better catalytic property for some chemical reactions. In another case, the nanochex will be favorable for some specific applications, such as electrochemical energy storage, especially Li ion batteries (LIBs), owing to the high surface area and direct contact with the conducting Ti foil.

In detailed observations, we often found that some nanochexes have nanowires as their fringes. Most importantly, these nanowires are only located along some specific edges. Just like what is revealed in Figures 3 and 4a,b, parallel to the specific direction, some nanowires are clearly detected, especially from the locally enlarged images (Figure 3b,d). The nanochex's schematic model is illustrated in Figure 4c so as to recognize this status better. To investigate the detailed information about this, we have collected all the possibly observed images through TEM observations. Two kinds of nanostructures have been detected, which are shown in Figure 4, panels d and e, respectively. In Figure 4d, we could find several segments are growing together into one integrated nanowire. The other image shown in Figure 4e reveals one fully grown nanowire. The crystal structure of the nanowire is characterized by HRTEM imaging. Figure 4f is a high-resolution TEM image taken from the circled region in Figure 4e. It can be determined that, along two vertical directions, the regular crystal spacing of 0.274 and 0.248 nm correspond to the interplanar distances of (002) and (200) planes of hexagonal MoN, respectively. These investigations have verified that the nanowire growing along the specific direction is single crystal in nature and its growth direction (axis direction) is [200]. Compared with the body section of MoN nanochex,

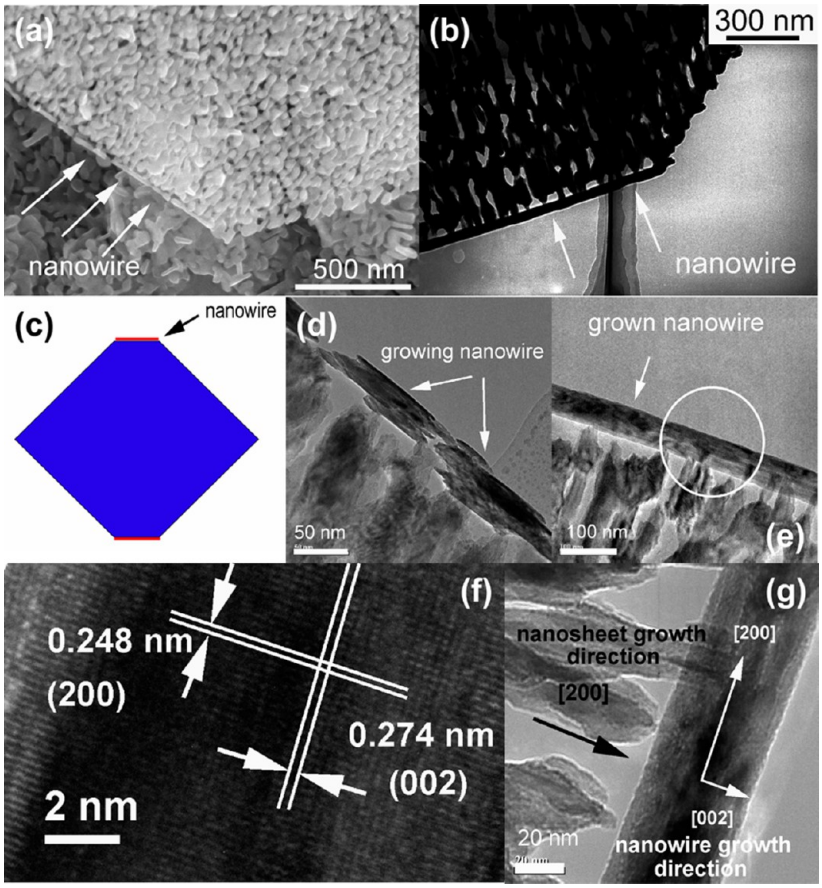

Figure 4. Detailed analysis for the hexagon-like MoN nanostructure. (a) SEM image; (b) TEM image. (c) Simulative model about the products. (d and e) Bright-field TEM images for the two different situations. (f) HRTEM image for the MoN nanowire marked in (e). (f) Black and white depiction for showing the different crystal orientation between the body-portion of hexagon-like MoN nanostructure and the subsequently grown MoN nanowire.

whose growth direction is also [200], in fact, the nanowire and the body section have different crystal orientation. All conclusions have been disclosed and highlighted in Figure 4g. So for the body section of MoN nanochex and the MoN nanowire located along the specific edge, presence of growing sequence should be possible. The whole growth process is probably as below: at the beginning, nanowires that make up the body section of MoN nanochex grow orientationally (Supporting Information). Afterward, parallel to the $[\bar{1}2\bar{2}]$ direction of the body section in hexagon-like MoN nanostructure, nanowire's segments appear and gradually grow into one total nanowire. To uncover the reason behind this fact, a series of control experiments have been carried out and enough data through SEM has been collected just like our previous work.[37,38] In Figure 5, panels a, b, c and d, and e are separately the SEM images for remaining 5, 10, 20, and 30 min at 850 °C with the same gas flux of 20 sccm NH_3 and 70 sccm N_2 and the same mixed powder of MoO_3 and Al in a molar ratio 1:4. From these images, the formation of the hexagon-like MoN nanostructure is suggested to be a process comprised of deoxidization, gasification, solidification, and orientational growth. The introduction of Al powder in the raw materials is to reduce the oxides into metal as given by

$$2Al(s) + MoO_3(s) \rightarrow Al_2O_3(s) + Mo(s) + \Delta(heat) \quad (1)$$

$$3MoO_3(s) + 2Al(s) \rightarrow Al_2O_3(s) + 3MoO_2(g) + \Delta(heat) \quad (2)$$

$$MoO_3(s) + \Delta(heat) \rightarrow MoO_3(g) \quad (3)$$

$$2MoO_3(g) + 4NH_3(g) \rightarrow 2MoN(s) + 6H_2O(g) + N_2(g) \quad (4)$$

$$6MoO_2(g) + 8NH_3(g) \rightarrow 6MoN(s) + 12H_2O(g) + N_2(g) \quad (5)$$

Formation of Al_2O_3 could produce much heat and make the central temperature higher than that around the location. Thereby a kind of kinetic control was made out which probably is very important during the subsequent fabrication.[39] In the first stage, sublimated MoO_3 or MoO_2 gas carried downstream by the high-pure N_2 and NH_3 reacts with NH_3 into MoN. Subsequently, MoN gas condenses and forms alloy-liquid clusters with Au atoms (Au film on Ti foil should melt and aggregate into nanoparticles under our experimental temperature) or is solidified through a gas−solid process without Au film coated on Ti foil.

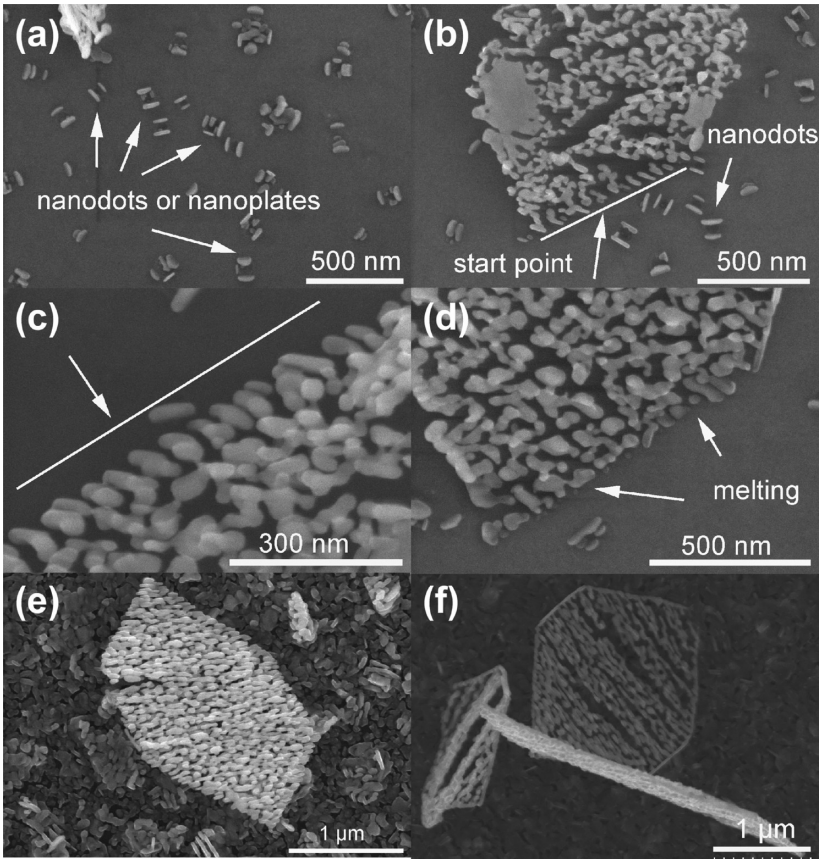

Figure 5. Time effect: SEM images for remaining (a) 5 min, (b) 10 min, (c and d) 20 min, and (e) 30 min at 850 °C with the same gas flux of 20 sccm NH_3 and 70 sccm N_2 and the same mixed powder of MoO_3 and Al in a molar ratio 1:4. According to above data, one process of gas phase self-assembly has been proposed. In the last growth stage (f), products are self-confined and achieved.

When the alloy-liquid clusters reach supersaturation, the nanodots or nanoplates of MoN appear Figure 5a. Under some proper conditions (maybe owing to the sheet-like structure of MoN (revealed in the later portion) and the surface tension between MoN and Ti foil), these nanoplates lie on the Ti foil regularly with the automatic style and serve as growing start-points (Figure 5b,c). Soon the start-points evolve into body portion of hexagon-like MoN nanostructure (Figure 5c). Finally, the start points melt together (Figure 5d) and nanowires are fabricated along the $[\bar{1}2\bar{2}]$ direction (Figure 5e,f).

From the whole growing process, a new self-assembly way has been discovered. Considering the loose structure and single crystalline in essence, we should conclude that the original regular arrangement of nanoplates or nanodots plays a crucial role in fabrication of MoN nanostructure. It is truly a self-assembly. Afterward, the MoN nanostructure grows in term of "self-confinement" style. According to this style, growth of MoN is limited in compressed hexagonal morphology. In wet chemistry, with the assistance of organic molecules or inorganic ions adsorption on special crystal planes, or with use of hard template, for example, AAO, confined growth has been achieved. However, our products have not experienced above-mentioned process. So it is a novel self-assembly way, which could be named "self-confinement process".

All the above investigations have shown an attractive MoN self-assembled nanostructure. This structure has complex texture, regular morphology and nature of single crystalline indeed. To seek for a reasonable explanation about the formation, an atomic schematic illustration of hexagonal MoN projected on (011) crystal plane is applied (Supporting Information). MoN crystal has a hexagonal structure with the space group of $P6_{3/mmc}$. For the (011) crystal plane of hexagonal MoN, the angle between $(11\bar{1})$ and $(\bar{2}1\bar{1})$ is about 83.8°. It is approximate to the acute angles of the nanochexes (Figure 2a and Supporting Information). Actually, most of nanochexes dispersed on TEM grid have the similar acute angles because they are ultrasonicated from Ti foil and mostly sleep horizontally on the carbon-coated grid film. However, due to the samples' tilt against the Ti foil, the real value of the acute angle in nanochex could not be exactly certified by SEM imaging indeed.

We suppose that structural merits of MoN are the driving force for the body section's oriented growth, which experiences a so-called "self-confinement

process". Along the outer fringe of the MoN nanochex, two parallel MoN nanowires grow along the specific direction with a different crystal orientation from the body section. In a word, the MoN nanochex we obtained has a novel and hierarchical structure, and what we should emphasize is that the unique nanochex is achieved by a self-assembly at gas−solid interface. Simulative model reveals all the crucial information about MoN nanochex, including morphologies, crystal planes, directions, angles, and nanowires orientation (Supporting Information). All these conclusions come from the data of SEM, TEM, HRTEM, and SAED. The appearance of the outer nanowires is optional. When the concentration of Mo source arises to some extent, some rhombus-like MoN is obtained, which is the result of MoN full growth (Supporting Information).

The formation of MoN nanochex could be explained by the hypothesis of system's energy minimization. From the crystal structure (Supporting Information), which is a projection of the crystal structure along [011], it is evident that the Mo and N atoms are alternatively arranged parallel to the [200]. So the (200) plane is terminated with either Mo or N atoms and has a net ionic charge on the surface (called polar surface, same to ZnO[8−13]). In gas−solid growth, polar plane initiates fast growth. However, along [11$\bar{1}$] and [$\bar{2}$1$\bar{1}$], we could find tha, Mo and N atoms are aligned evenly. So these planes are neutral surfaces and the most typical low-energy facets.[40,41] In MoN nanochex's growth, the first step is that MoN grows rapidly along [200] direction, and at the same time, along [$\bar{1}$2$\bar{2}$] or its equivalent direction. Once (11$\bar{1}$) and ($\bar{2}$1$\bar{1}$) planes are achieved, the top parts would melt and be integrated. When the temperature is high enough or the MoO_3/Al molar ratio is raised, thermodynamic controls can be realized. In this status, rhombus MoN nanostructures will be acquired, due to the reason for enlarging the surfaces of (11$\bar{1}$) and ($\bar{2}$1$\bar{1}$) and leading to the formation of sides that are dominated by (11$\bar{1}$) and ($\bar{2}$1$\bar{1}$) surfaces. But when the reaction temperature is lower and MoO_3/Al molar ratio is down to some extent, kinetic controls are realized. In this condition, growing rate along [$\bar{1}$2$\bar{2}$] is faster than that of [200]. So when the equivalent planes of (11$\bar{1}$) and ($\bar{2}$1$\bar{1}$) are formed on the opposite sides of MoN nanochex, (200) crystal planes are still present. Aiming at lowering the surface energy of (200), nanowires parallel to [200] begin to grow. Polar surfaces are usually supposed to be chemically active and facile to trigger materials growing.[8−13] The deduction has been verified again in our synthesis of MoN nanochex. The whole growth process could be described as a "self-confinement process", and now it is being extended to other materials' designed synthesis, such as Mo^2C, *etc.*

In view of the crystal structure, as we know, there are great amounts of naturally or artificially synthesized materials possessing layered (or sheet-like) crystal structures, such as layered asbestos, chrysotil, brucite minerals, graphite, P, As, Sb, Bi, NbS_2, GaSe, MoS_2, *etc.* and inorganic-surfactant lamellar mesostructured materials.[42] As for hexagonal MoN, from its atomic schematic model (Supporting Information), we could determine that it also possesses natural sheet-like structure. Along [002], [200], [020] and their equivalent directions (Supporting Information), the hexagonal MoN could be separated into different segments. As the evidence for the deduction, some sheet-like structures can be clearly detected at the end of the nanowires (Figure 4g).

As is mentioned above, MoN is a multifunctional material and can find many applications in catalysis, industrial sensing and polishing. However, it is scarcely reported in the fields of energy storage and conversion. Recently, MoN nanostructures, *e.g.*, nanobelt, nanoparticles, and thin film, have been generated and applied in LIBs.[43,44] Transition metal nitrides are intriguing anode materials in LIBs, because of their low production cost, good structural stability, high electrical conductivity and low volume change in lithiation and delithiation.[45−47] In this regard, we can not only harvest the MoN nanochex with regular mesoporous structure and single crystallinity, but also successfully erect them on Ti foil in one step, so that a gate for direct use of them in LIBs has been opened. The detailed discussions about the outstanding electrochemical performances are displayed in the Supporting Information. All the characterizations presented in Figure S1 greatly improved electrochemical energy storage performance for the synthesized MoN nanochexes array on Ti foil, especially compared to the randomly dispersed MoN particles, where the much poorer Li-storage performance and much higher inner resistance are verified (Supporting Information). The enhanced electrochemical energy storage performance is believed to derive from the unique architecture and structure of MoN nanochexes array. First, the porous structure can strengthen the contact between the active material and electrolyte, and thereby will be favorable for the rapid exchange of Li ions among them. Second, the nanochexes array is very suitable for electrolyte's diffusion and penetration when cycling. Third, the direct contact between the MoN nanochexes and conductive substrate of Ti foil will accelerate the charge transfer. All the three aspects, of course, can help to confirm the claims of the enhanced electrochemical energy storage performance from the nanochexes array.

CONCLUSIONS

In summary, hexagon-like MoN hierarchical nanostructure, namely nanochex, which is composed of textured single-crystal nanowires, has been successfully synthesized by both aluminothermal reactions and steady-state turbulent gas flow controls. The

as-synthesized MoN nanostructure normally has a size distribution of 2−4 μm, and could be tailored in morphology, size, thickness, *etc.* The formation mechanism of the MoN nanochex is proposed based on the characters of hexagonal MoN's crystal structure and the hypothesis of minimizing the system's energy. This research result would be meaningful to dig out the origin of self-assembly in gas−solid phase, and meanwhile, the synthesis strategy applied here can also be extended to many other materials, *e.g.*, nitrides, carbides, even borides, *etc.* and thereby to significantly tailor their resulting architectures and properties. In its application in LIBs, the MoN nanochex exhibits an enhanced efficiency of electrochemical energy storage and the deliverable capacity can be stable at 720 mAh/g with an attractive Coulombic efficiency of 98.5%, providing a promising candidate for the electrode materials of superior secondary LIBs.

MATERIALS AND METHODS

Synthesis of MoN Nanochex. The synthesis of MoN hexagon-like nanostructure was carried out in a horizontal tube furnace through a temperature-programmed procedure. The precursor, mixed powder of MoO_3 and Al with a molar ratio of 1:1−1:4 was put in the front of an alumina boat, and a piece of Ti foil (8 mm × 8 mm) coated with nothing or a thin gold layer of 10−20 nm in thickness was placed behind the mixed powder by a separation of 0.2−0.3 cm in the boat. Then, the alumina boat was carefully put into the horizontal tube furnace and located in the constant-temperature zone. Diameter of the quartz tube is about 3 cm. The system was obturated, and high-pure N_2 (100 standard cubic centimeters per minute, sccm) was introduced into the reactor to expel air before reaction. About 10 min later, the N_2 flow was switched into 30 sccm and the system temperature was raised from room-temperature to 850 °C (varying from 820 to 880 °C, normally 850 °C) with a heating rate of 20 °C/min under ambient pressure. Afterward, 20 sccm NH_3 and 70 sccm high pure N_2 were separately introduced into the CVD system by a three-way valve. The Ti foil was kept in the highest temperature for 30 min, and was cooled down to room-temperature naturally in 30 sccm high-pure N_2. The acquired Ti foil was covered with something blue.

Materials Characterization. Powder X-ray diffraction (XRD) patterns of the products (located on original Ti foil) was recorded on a Rigaku D/MAX-200 diffractometer (Japan) using Cu Kα (λ = 1.524 Å) radiation at a scanning rate of 8°/min, 40 kV and 100 mA. The samples were directly brought to morphology observations by SEM (S-4800, Hitachi, Japan) and ultrasonicated in alcohol for several minutes dispersing onto amorphous carbon-coated copper grid for TEM analysis (TEM, 200CX, 160 kV, JEOL; High-resolution TEM (HRTEM), Tecnai F30, 300 kV, Philips). Selected-area electron diffraction (SAED) and energy-dispersive X-ray spectrometry (EDS, an accessory to F30) were utilized to characterized the detailed microstructures and compositions of the products.

Electrochemical Characterization. Prior to actual test, bare Ti foil was first cut into smaller pieces with size of 0.4 × 0.4 cm^2 and weighed in a high-precision analytical balance (Sartorius, max weight 5100 mg, d = 0.001 mg). The pieces of Ti foil with MoN nanochexes array covered were then synthesized and weighed in the same balance. Through this way, the exact sample mass used for Li-ion batteries testing was available. Afterward, the obtained samples were used as electrodes with 1 M $LiPF_6$ in ethylene carbonate and diethyl carbonate (EC-DEC, v/v = 1:1) as electrolyte. Celgard 2400 was used as the separator film to isolate the two electrodes. Pure Li foil (99.9%, Aldrich) was accepted to server as counter electrode and reference electrode. The swagelok cell was assembled in an argon-filled glovebox where moisture and oxygen concentrations were strictly limited below 0.1 ppm. The electrochemical tests were performed on Neware Battery Testing System in the model of 5 V5 mA and cyclic voltammetry (CV) was collected using Autolab (model of AUT71740). The covered samples on Ti foils were calculated to be ranging from 0.6 to 0.9 mg/cm^2.

Conflict of Interest: The authors declare no competing financial interest.

Supporting Information Available: Experimental methods for synthesis of MoN nanochex, materials' and electrochemical characterizations; additional structural characterization of MoN nanochex; various effects in formation of the MoN nanochex. The Supporting Information is available free of charge on the ACS Publications website at DOI: 10.1021/acsnano.5b02415.

Acknowledgment. This work was financially supported by the Thousand Young Talents Program of the Chinese Central Government (Grant No. 0220002102003), National Natural Science Foundation of China (NSFC, Grant No. 21373280, 21403019, 51121091, 21133001, 21261130090, 21228301), MOST (2011CB808702), Beijing National Laboratory for Molecular Sciences (BNLMS), the Fundamental Research Funds for the Central Universities (0301005202017) and Hundred Talents Program at Chongqing University (Grant No. 0903005203205).

REFERENCES AND NOTES

1. Hu, J. T.; Odom, T. W.; Lieber, C. M. Chemistry and Physics in One Dimension: Synthesis and Properties of Nanowires and Nanotubes. *Acc. Chem. Res.* **1999**, *32*, 435–445.
2. Xia, Y.; Yang, P.; Sun, Y.; Wu, Y.; Mayers, B.; Gates, B.; Yin, Y.; Kim, F.; Yan, H. One-Dimensional Nanostructures: Synthesis, Characterization, and Applications. *Adv. Mater.* **2003**, *15*, 353–389.
3. Goldberger, J.; He, R.; Zhang, Y.; Lee, S.; Yan, H.; Choi, H.-J.; Yang, P. Single-Crystal Gallium Nitride Nanotubes. *Nature* **2003**, *422*, 599–602.
4. Wang, Z.-X.; Schleyer, P. v. R. Construction Principles of "Hyparenes": Families of Molecules with Planar Pentacoordinate Carbons. *Science* **2001**, *292*, 2465–2469.
5. Hurst, S. J.; Payne, E. K.; Qin, L.; Mirkin, C. A. Multisegmented One-Dimensional Nanorods Prepared by Hard-Template Synthetic Methods. *Angew. Chem., Int. Ed.* **2006**, *45*, 2672–2692.
6. Lin, Y.; Boker, A.; He, J.; Sill, K.; Xiang, H.; Abetz, C.; Li, X.; Wang, J.; Emrick, T.; Long, S.; Wang, Q.; Balazs, A.; Russell, T. P. Self-Directed Self-Assembly of Nanoparticle/Copolymer Mixtures. *Nature* **2005**, *434*, 55–59.
7. Velev, O. D. Self-Assembly of Unusual Nanoparticle Crystals. *Science* **2006**, *312*, 376–377.
8. Lauhon, L. J.; Gudiksen, M. S.; Wang, D.; Lieber, C. M. Epitaxial Core-Shell and Core-Multishell Nanowire Heterostructures. *Nature* **2002**, *420*, 57–61.
9. Lao, J. Y.; Wen, J. G.; Ren, Z. F. Hierarchical ZnO Nanostructures. *Nano Lett.* **2002**, *2*, 1287–1291.
10. Gao, P. X.; Wang, Z. L. Mesoporous Polyhedral Cages and Shells Formed by Textured Self-Assembly of ZnO Nanocrystals. *J. Am. Chem. Soc.* **2003**, *125*, 11299–11305.
11. Wang, Z. L.; Pan, Z. W. Junctions and Networks of SnO Nanoribbons. *Adv. Mater.* **2002**, *14*, 1029–1032.
12. Jun, Y.-w.; Lee, S.-M.; Kang, N.-J.; Cheon, J. Controlled Synthesis of Multi-Armed CdS Nanorod Architectures Using Monosurfactant System. *J. Am. Chem. Soc.* **2001**, *123*, 5150–5151.

13. Dick, K. A.; Deppert, K.; Larsson, M. W.; Martensson, T.; Seifert, W.; Wallenberg, L. R.; Samuelson, L. Synthesis of Branched 'Nanotrees' by Controlled Seeding of Multiple Branching Events. *Nat. Mater.* **2004**, *3*, 380–384.
14. Jiang, S. P.; Liu, Z.; Tian, Z. Q. Layer-by-Layer Self-Assembly of Composite Polyelectrolyte−Nafion Membranes for Direct Methanol Fuel Cells. *Adv. Mater.* **2006**, *18*, 1068–1072.
15. Liu, B.; Zeng, H. C. Fabrication of ZnO "Dandelions" *via* a Modified Kirkendall Process. *J. Am. Chem. Soc.* **2004**, *126*, 16744–16746.
16. Liu, B.; Zeng, H. C. Mesoscale Organization of CuO Nanoribbons: Formation of "Dandelions". *J. Am. Chem. Soc.* **2004**, *126*, 8124–8125.
17. Dujardin, E.; Hsin, L.-B.; Wang, C. R. C.; Mann, S. DNA-Driven Self-Assembly of Gold Nanorods. *Chem. Commun.* **2001**, 1264–1265.
18. Kim, F.; Kwan, S.; Akana, J.; Yang, P. Langmuir−Blodgett Nanorod Assembly. *J. Am. Chem. Soc.* **2001**, *123*, 4360–4361.
19. Li, M.; Schnablegger, H.; Mann, S. Coupled Synthesis and Self-assembly of Nanoparticles to Give Structures with Controlled Organization. *Nature* **1999**, *402*, 393–395.
20. Yang, H.; Coombs, N.; Ozin, G. A. Morphogenesis of Shapes and Surface Patterns in Mesoporous Silica. *Nature* **1997**, *386*, 692–695.
21. Zhao, D.; Sun, J.; Li, Q.; Stucky, G. D. Morphological Control of Highly Ordered Mesoporous Silica SBA-15. *Chem. Mater.* **2000**, *12*, 275–279.
22. Yin, J. S.; Wang, Z. L. Ordered Self-Assembling of Tetrahedral Oxide Nanocrystals. *Phys. Rev. Lett.* **1997**, *79*, 2570–2573.
23. Braun, P. V.; Osenar, P.; Stupp, S. I. Semiconducting Superlattices Templated by Molecular Assemblies. *Nature* **1996**, *380*, 325–328.
24. Sun, S.; Murray, C. B.; Weller, D.; Folks, L.; Moser, A. Monodisperse FePt Nanoparticles and Ferromagnetic FePt Nanocrystal Superlattices. *Science* **2000**, *287*, 1989–1992.
25. Toth, L. E. *Transition Metal Carbides and Nitrides*; Academic Press, New York, 1971.
26. Volpe, L.; Boudart, M. Ammonia Synthesis on Molybdenum Nitride. *J. Phys. C* **1986**, *90*, 4874–4877.
27. Nagai, M.; Miyao, T. Activity of Alumina-supported Molybdenum Nitride for Carbazole Hydrodenitrogenation. *Catal. Lett.* **1992**, *15*, 105–109.
28. Nagai, M.; Miyao, T.; Tuboi, T. Hydrodesulfurization of Dibenzothiophene on Alumina-Supported Molybdenum Nitride. *Catal. Lett.* **1993**, *18*, 9–14.
29. Neylon, M. K.; Choi, S.; Kwon, H.; Curry, K. E.; Thompson, L. T. Catalytic Properties of Early Transition Metal Nitrides and Carbides: N-butane Hydrogenolysis, Dehydrogenation and Isomerization. *Appl. Catal., A* **1999**, *183*, 253–263.
30. Papaconstantopoulos, D. A.; Pickett, W. E. Effects of Disorder on High-Temperature Superconductivity in Cubic MoN. *Phys. Rev. B* **1985**, *31*, 7093–7097.
31. Wang, S.; Wang, X.; Zhang, Z.; Qian, Y. Synthesis of Nanocrystalline MoN from A New Precursor by TPR Method. *J. Mater. Sci.* **2003**, *38*, 3473–3478.
32. Anitha, V. P.; Vitta, S.; Major, S. Structure and Properties of Reactivity Sputtered γ-Mo_2N Hard Coatings. *Thin Solid Films* **1994**, *245*, 1–3.
33. Rudnik, P. J.; Graham, M. E.; Sproul, W. D. High Rate Reactive Sputtering of MoNx Coatings. In *Metallurgical Coatings and Thin Films 1991*; McGuire, G. E., McIntyre, D. C., Hofmann, S., Eds.; Elsevier: Oxford, 1991; pp 293−297.
34. Choi, J.-G.; Choi, D.; Thompson, L. T. Preparation of Molybdenum Nitride Thin Films by N^+ Ion Implantation. *J. Mater. Res.* **1992**, *7*, 374–378.
35. Donovan, E. P.; Hubler, G. K.; Mudholkar, M. S.; Thompson, L. T. Ion-Beam-Assisted Deposition of Molybdenum Nitride Films. *Surf. Coat. Technol.* **1994**, *66*, 499–504.
36. Wu, J. D.; Wu, C. Z.; Song, Z. M.; Wu, L. H.; Li, F. M. Synthesis of Molybdenum Nitride γ-Mo_2N by Multipulse Laser Irradiation of Molybdenum in Nitrogen. *Appl. Surf. Sci.* **1995**, *90*, 81–87.
37. Wang, Y.; Wu, K. As a Whole: Crystalline Zinc Aluminate Nanotube Array−Nananet. *J. Am. Chem. Soc.* **2005**, *127*, 9686–9687.
38. Wang, Y.; Liao, Q.; Lei, H.; Zhang, X. P.; Ai, X. C.; Zhang, J. P.; Wu, K. Interfacial Reaction Growth: Morphology, Composition, and Structure Controls in Preparation of Crystalline ZnxAlyOz Nanonets. *Adv. Mater.* **2006**, *18*, 943–947.
39. Wang, Y.; Chen, J.; Liao, Q.; Sun, W.; Li, J. L.; Zhang, J. P.; Wu, K. Bifilar Helix-like Nanobelt of Single Crystalline Zn_2SnO_4 Fabricated by Aluminothermal Reaction Approach. *Acta Phys. Chim. Sin.* **2012**, *28*, 2500–2506.
40. Cao, M.; Liu, T.; Gao, S.; Sun, G.; Wu, X.; Hu, C.; Wang, Z. L. Single-Crystal Dendritic Micro-Pines of Magnetic α-Fe_2O_3: Large-Scale Synthesis, Formation Mechanism, and Properties. *Angew. Chem., Int. Ed.* **2005**, *44*, 4197–4201.
41. Wang, Z. L.; Kong, X. Y.; Zuo, J. M. Induced Growth of Asymmetric Nanocantilever Arrays on Polar Surfaces. *Phys. Rev. Lett.* **2003**, *91*, 185502–185508.
42. Li, Y. D.; Li, X. L.; He, R. R.; Zhu, J.; Deng, Z. X. Artificial Lamellar Mesostructures to WS_2 Nanotubes. *J. Am. Chem. Soc.* **2002**, *124*, 1411–1416.
43. Nandi, D. K.; Sen, U. K.; Choudhury, D.; Mitra, S.; Sarkar, S. K. Atomic Layer Deposited Molybdenum Nitride Thin Film: A Promising Anode Material for Li Ion Batteries. *ACS Appl. Mater. Interfaces* **2014**, *6*, 6606–6615.
44. Park, H.-C.; Lee, K.-H.; Lee, Y.-W.; Kim, S.-J.; Kim, D.-M.; Kim, M.-C.; Park, K.-W. Mesoporous Molybdenum Nitride Nanobelts as an Anode with Improved Electrochemical Properties in Lithium Ion Batteries. *J. Power Sources* **2014**, *269*, 534–541.
45. Panabière, E.; Emery, N.; Bach, S.; Pereira-Ramos, J. P.; Willmann, P. Ball-Milled Li_7MnN_4: An Attractive Negative Electrode Material for Lithium-Ion Batteries. *Electrochim. Acta* **2013**, *97*, 393–397.
46. Song, T.; Kil, K. C.; Jeon, Y.; Lee, S.; Shin, W. C.; Chung, B.; Kwon, K.; Paik, U. Nitridated Si−Ti−Ni Alloy as an Anode for Li Rechargeable Batteries. *J. Power Sources* **2014**, *253*, 282–286.
47. Sun, Q.; Fu, Z.-W. An Anode Material of CrN for Lithium-Ion Batteries. *Electrochem. Solid-State Lett.* **2007**, *10*, A189–A193.